3B.3 ENSEMBLE KALMAN FILTER ASSIMILATION OF DOPPLER RADAR DATA: ANALYSES OF A DEVELOPING MCS

Michael C. Coniglio[1,2], David C. Cowell[3], and Louis J. Wicker[1]

[1]University of Oklahoma/Cooperative Institute for Mesoscale Meteorological Studies, Norman, Oklahoma
[2]NOAA/OAR/National Severe Storms Laboratory, Norman, Oklahoma
[3]National Center for Atmospheric Research, Boulder, Colorado

1. INTRODUCTION

Snyder and Zhang (2003; SZ03 hereafter) introduced the storm-scale NWP community to the use of an Ensemble Kalman Filter (EnKF) (Evensen 1994) for assimilating Doppler radar observations into numerical models, which has been used to analyze observed isolated supercell thunderstorms (Dowell et al. 2004; D04 hereafter). D04 noted that the technique showed promise in depicting the reflectivity and velocity structures of the supercell, but seemed to be lacking in retrieving the thermodynamic variables and the surface cold pool in particular. Furthermore, it is noted in SZ03 and D04 that the utility of the EnKF technique applied to storm-scale problems is unknown in complex convective situations with multiple updrafts and interacting cold outflows, which is related to the linearity and normality assumptions of the technique. Therefore, it is unclear how well the technique will work on observed mesoscale convective systems (MCSs); it is well known that MCSs depend on the character of the convectively generated cold pool and often develop from a complex interaction of mixed convective modes. Therefore, the goal of this study is to examine the application of the EnKF technique using real Doppler radar observations of a developing MCS. Storm-scale EnKF is in a developmental stage and, therefore, we focus on examining the viability of the technique for a complex convective scenario and present some simple experiments that highlight the sensitivity of the analyses to aspects of the filter design.

2. ENKF RADAR DATA ASSIMILATION

The EnKF is a method to retrieve unobserved atmospheric variables from observations, which in this application is Doppler radar reflectivity and radial velocity. Statistical assimilation techniques require information on the relationship (or covariance) between the unobserved variables and the observed variables. The EnKF obtains these covariances from an ensemble of numerical model forecasts, which is presumably a benefit of using this technique over 3D or 4D variational schemes since the latter requires the covariance relationships to be prescribed before hand. Given an observation, the goal is to adjust the other model variables according to the covariance between the model reflectivity at that point and the unobserved model variables near the observation location. For example, given a reflectivity observation of 50 dBZ, we want to adjust the vertical velocity in the model forecasts based on this observation. We find the covariance between the model's representation of reflectivity at the observation point and the vertical velocity at the grid points near the observation point among all the ensemble members. If there is a positive relationship between reflectivity and vertical velocity and the observed reflectivity is higher than the ensemble mean reflectivity prior to the observation, then the adjustments will result in a mean vertical velocity that is higher than the ensemble mean prior to the observation. This procedure is repeated for every model variable (except for pressure and the mixing coefficient) and for every observation. We refer the interested reader to SZ03 and D04 for further details of the EnKF technique and its application to radar data.

3. MCS OBSERVATIONS

This study examines the 16-17 June 2005 MCS across southeast Kansas and northwest Oklahoma. The environment near initiation had 0-6 km bulk wind shear of 40 kt, mixed-layer CAPE of 3500 J kg^{-1}, and downdraft CAPE of 1400 J kg^{-1} (Fig. 1). The convection developed quickly into a cluster of supercells and multicells and later organized into a derecho-producing MCS (Johns and Hirt 1987). Although a long-term goal of storm-scale data assimilation and NWP is to be able to predict the entire evolution of events of this type, this study focuses on EnKF analyses of the developing MCS in the time period between 2300 UTC on 16 June and 0030 UTC on 17 June.

The period of Doppler radar observations consists of multiple cells with various modes undergoing an upscale transition. A benefit of the relatively large size of the developing MCS is that data was collected from both the WSR-88D sites at Dodge City, KS (KDDC) and at Vance Air Force Base in Oklahoma (KVNX). Although data from both these radars could be used in the assimilation, only the KDDC data is used in this capacity. This affords the use of the KVNX data as independent evaluation, especially in later stages of the MCS development when the system is located nearly half way between the two radar sites and has a convective organization nearly perpendicular to the beams of both radars. The Oklahoma Mesonet surface-observing site at Buffalo, OK also is used in the evaluation.

4. NUMERICAL MODEL AND ENSEMBLE DESIGN

The numerical forecast model employed is the collaborative model for multiscale atmospheric simulation (COMMAS). Prognostic variables include the three velocity components, *u, v*, and *w*, pressure (in the form of the perturbation Exner function, π'), potential temperature, θ, and six categories of water substance, including water vapor, q_v, cloud water, q_c, rain water, q_r, ice, q_i, snow, q_s, and hail/graupel, q_h. A Lin-Farley-Orville scheme is used for the microphysical parameterization with parameters set to bias the distribution to a mixture of hail and graupel. More details on the model can be found in Coniglio et al. (2006).

The model domain contains 108 x 78 x 31 grid points covering 321 km x 231 km x 18 km in the *x, y*, and *z* directions, respectively, with grid intervals of 3 km in the horizontal directions and a vertically stretched grid with a constant interval of 400 m in the lowest 5 layers stretching to 700 m at the top of the domain. Although this model resolution can only represent the gross features of convective cells accurately, it is suitable for studying MCSs (Weisman et al. 1997, Bryan et al. 2003) and is comparable to the state-of-the-art operational NWP models (Kain et al. 2006).

An ensemble of 50 horizontally homogeneous model states is created by adding uncorrelated random perturbations to the base-state environment represented in Fig. 1. This initialization technique differs from that of D04 in that perturbations vary only in the vertical direction. Unless otherwise noted, the standard deviation (σ, or referred to as the "spread") of the perturbations applied to *u* and *v* among the 31 vertical levels is specified to be 2.0 m s^{-1}. In addition, perturbations with $\sigma = 1$ K are added to the temperature and dewpoint profiles. The perturbations result in a standard deviation of CAPE of 333 J kg^{-1} and 0-6 km bulk shear of 2.4 m s^{-1} among the 50 initial states, which is comparable to the accuracy provided by the observations and the RUC analysis.

5. ENKF ANALYSES

a. Configuration of the control and baseline experiments

A control experiment (CNTL) is produced using the initialization procedure described above. To facilitate the development of storms, ellipsoidal θ perturbations ("bubbles") of 2.5 K at the center that decrease to zero at a horizontal (vertical) radius of 10 km (5 km) are introduced every five minutes near the locations where the difference between the observed and ensemble mean reflectivity field exceeds 30 dBZ. Although the bubbles are additive in locations where they overlap, we use a large dBZ difference and place the bubbles randomly around these locations to prevent too many bubbles from piling up large temperature perturbations that could lead to model instabilities. We also find that distributing the bubbles randomly near these locations helps to maintain ensemble spread during the assimilation compared to simply placing bubbles at the exact locations where the reflectivity is too low.

Spread in the ensemble also is maintained by adding spatially smoothed noise every five minutes to *u*, *v*, and θ, with a standard deviation of 1 m s^{-1} and 0.5 K, respectively, at locations where the observed reflectivity exceeds 20 dBZ. For this we use the technique in Caya et al. (2005) (see their section 3b1). Through experimentation, it is found that these techniques maintain enough spread throughout the 90 minute assimilation period to preclude any substantial benefit from artificial covariance inflation (Anderson 2001, Tong and Xue 2005), which is not used in any of the assimilation experiments.

One of the goals of storm-scale EnKF is to produce a scale-appropriate analysis of the convective event in question. It is important to show that an EnKF analysis can improve significantly upon a simulation that is produced using traditional techniques, e.g. using warm bubbles to initiation convection. Therefore, we compare the CNTL experiment to a baseline experiment (BASE), which is one that we'd hope to significantly improve upon using the EnKF technique. The purpose of the BASE experiment is to show that the improvement provided by using EnKF is obvious and substantial.

Warm bubbles are introduced in the BASE experiment where the difference between the observed reflectivity and model reflectivity exceeds 30 dBZ. However, no assimilation of radar data takes place and the bubbles are placed at the exact locations of where the storms are missing in the model (remember that the bubbles are placed randomly around these locations in the CNTL experiment). Bubbles are introduced every five minutes and the maximum potential temperature perturbation at any grid point is limited to 6 K. It is hoped that the assimilation of radar data over this time period can improve on the performance of this rather simple baseline ensemble.

b. Comparison of CNTL and BASE reflectivity

The CNTL experiment depicts three main storm clusters in the correct locations after 20 minutes of assimilation (about 5 volume scans) (Figs. 2a & b), but the storms are slightly smaller and less intense than in reality. By 40 minutes however, the size of the storm clusters closely match reality with a slight under representation of the maximum reflectivity values (see Fig. 4 for a comparison of the overall mean error in reflectivity). This trend continues throughout the assimilation period with the general storm-scale configuration represented very accurately in the CNTL experiment. Note the supercell structures evident in the observations and in the analysis.

In general, the EnKF system appears to require about 5-6 volume scans to reproduce the size and strength of the cells. For example, notice the small, newly developed cell almost due east of KDDC at 40 min (circled on Fig. 2d). The EnKF procedure hasn't had time to represent the cell in the analysis valid at the same time (area circled Fig. 2e), but very accurately represents this cell at 40 minutes (circled in Figs. 2g and 2h).

A comparison of the CNTL and BASE experiments (Figs. 2c, 2f, 2I, and 2l) clearly illustrates the benefit of EnKF versus a bubble-only approach. The storms are much slower to develop in the BASE experiment and, furthermore, lack the storm scale detail and accurate placement of the storms in the CNTL experiment. This increase in the storm-scale detail extends to other variables as well (not shown). Additionally, the CNTL experiment comes much closer to matching the evolution of the surface conditions observed at the Buffalo, OK Mesonet site (Fig. 3; the results for the BASE experiment are not shown). The storm-scale evolution of *u*, temperature, and dewpoint are represented fairly well (Fig. 3), although the drying is too large and the cooling is too small in the ensemble mean (the *v* component is not represented well, partially because the cold pool is too fast in the model simulations).

Statistics to evaluate the experiments are calculated using the observed radial velocity and reflectivity from the KVNX radar. Measures include the root mean square (rms) difference between the observations and the ensemble mean, the standard deviation (spread) of the ensemble, and the mean difference (bias) between the observations and the ensemble. Although this evaluation doesn't account for differences in measuring characteristics between the KDDC and KVNX radars, this provides a reasonably accurate means to evaluate the overall quality of the analyses with independent measurements. In addition to the standard measures, we provide information on the so-called consistency check of the ensemble (SZ03, D04). In simple terms, this states that the EnKF technique is optimal if the sum of the specified observation error variance and the ensemble variance approaches the mean squared error when averaged over all observations at a given time. The consistency check is shown as a ratio of the total variance to the mean squared error; a value approaching one indicates a well-configured ensemble.

The 90-minute assimilation of KDDC data starting at 2300 UTC produces an analysis that significantly improves the *rms* compared to BASE for both radial velocity and reflectivity especially (Figs. 4 and 5), even though the storms are not introduced at their exact locations in the CNTL experiment. This is indicative of the positive covariances between reflectivity and vertical motion that develop relatively quickly, which allow the EnKF procedure to develop the storms in the correct locations faster than simply placing warm bubbles at the storm locations periodically. Also note that the CNTL assimilation experiment is well configured in terms of reproducing the reflectivity fields as the consistency check approaches one after about 70 minutes of assimilation. However, the consistency check is significantly lower for the radial velocity, indicating a lack of spread or that the assumed observational error of 2.0 m s^{-1} is too small.

c. Sensitivity experiments

An important consideration in EnKF applications is the number of grid points to update and the weighting applied to the updates. Typically an elliptical influence region is specified around the observation location with a functional form described by Gaspari and Cohn (1999). As stated before, the update of a given model variable is proportional to the covariance between the model's representation of the observation and the nearby model variables. This influence region, or localization as it is often termed, defines which model variables are nearby, i.e, the covariance that is used to update the model variables is computed using all grid points inside this influence region. However, the covariance is scaled according to the distance of the grid point from the observation location. This scaling decreases smoothly from 1 at the observation location to 0 at the edge of the influence region. The CNTL experiment uses a region with a horizontal radius of 10 km and a vertical radius of 5 km. However, the optimal way to define this region for storm-scale applications has yet to be determined. Therefore, we also examine the sensitivity and implications of varying both the size of this region and the number of grid points that are updated within this region.

We first examine the sensitivity of the results to the choice of horizontal localization. Using a value of both 20 km and 5 km (versus the 10 km used in the CNTL experiment) does not significantly alter the overall statistical behavior (Fig. 6). This is confirmed by comparing the reflectivity and radial velocity structures between these two runs and the CNTL experiment (not shown). The *rms* is slightly worse for the 20 km experiment, but the most significant difference is in the spread, with an increase (decrease) in the localization radius causing a decrease (increase) in the spread. This suggests the localization radius may be a simple way to tune the ensemble to achieve the proper spread, at least for the observed variable. Additionally, the fact that the analysis of the storms does not change significantly with a change in the localization raises the question of the significance of the covariances, i.e., this raises the question, how often are we adjusting the model to noise? This could have important implications for the practical application and understanding the behavior of the EnKF technique.

We examine this behavior in several experiments that hold the horizontal localization threshold at 10 km, but only update the model variables if the covariance is above a certain threshold (we use correlation to define the threshold). We performed eight experiments in which we vary this threshold from 0.1 to 0.8 in increments of 0.1. For example, for an experiment with a correlation threshold of 0.2, only the model variables within the localization radius that are linearly correlated to the observation type at greater than or equal to 0.2 are adjusted.

The experiments with a threshold of 0.2 (COR2), 0.4 (COR4), 0.6 (COR6), and 0.8 (COR6) are examined in Figs. 7-9. As the correlation threshold increases, the average number of grid points that get adjusted decreases exponentially. In particular, the number of grid points adjusted in experiment COR6 is generally a factor of 10 less than the number of grid points adjusted in experiment COR2 (Fig. 7). It is interesting then to see that the differences in the reflectivity analyses between these two simulations are negligible (c.f. figs. 8 and 9). Differences in most of the non-observed variables between the CNTL run and COR2 also are negligible. Additionally, the structure and magnitude of the updrafts and downdrafts do not change substantially until the threshold increases to about 0.5. However, significant differences in the surface perturbation potential temperature and water vapor fields can be found once the threshold increases to 0.3-0.4 (not shown). In general, the maximum deficits and the spatial coverage of these perturbations decrease by 20-50% as the threshold increases from 0.2 to 0.6. Without detailed observations, it isn't clear which of these ensembles are performing best. Figure 3 shows that an ensemble that decreases the drying at the surface underneath the convection may be more realistic and, therefore, the COR4 and COR6 experiments may be better. However these runs also have a warmer cold pool, which was perhaps too warm to begin with (see Fig. 3, bottom left panel). Nonetheless, these results serve to show that simply changing how the covariances are defined can make large differences in the interpretation of the results and the retrieval of the non-observed variables. Although more work is needed, an encouraging sign is that using a lower threshold of 0.2-0.3 seems to make negligible differences in the structure, location, and magnitude of the storm-scale features, which can allow a substantial decrease in computational time.

6. SUMMARY AND FUTURE WORK

This study examines the utility of storm-scale EnKF data assimilation applied to a developing MCS. It is not clear how a technique that is optimal for Gaussian statistics will perform in such a highly nonlinear convective scenario. Results show that the EnKF appears as promising in its application to mixed mode and complex convective events as it does to isolated supercells (D04). The technique requires about 30-40 minutes of reflectivity and radial velocity data (about 5-6 volume scans) to accurately reproduce the storm-scale structure of the developing MCS. A problem found in past studies of storm-scale EnKF that spread is often deficient (SZ03), does not appear to be as much of a problem in this case, as the sum of the specified observation error variance and the ensemble variance approaches the mean squared error for the control simulation.

Sensitivity studies show, however, that the ensemble spread and the magnitude and structure of the non-observed variables can be modified significantly simply by changing how the localization is defined and the level of correlation allowed in the EnKF update step. Research is ongoing to further quantify these differences and to work toward understanding the structure of the covariances.

6. REFERENCES

Anderson, J. L., 2001: An ensemble adjustment filter for data assimilation. *Mon. Wea. Rev*., **129**, 2884-2903.

Bryan, G. H., J.C. Wyngaard, and J.M. Fritsch, 2003: Resolution requirements for the simulation of deep moist convection**.** *Mon. Wea. Rev.,* 131, 2394–2416.

Caya, A., J. Sun, and C. Snyder, 2005: A comparison between the 4DVAR and the Ensemble Kalman Filter Technique for Radar Data Assimilation. *Mon. Wea. Rev*., **133**, 3081-3094.

Coniglio, M.C., D.J. Stensrud, and L.J. Wicker, 2006: Effects of upper-level shear on the structure and maintenance of strong quasi-linear mesoscale convective systems. *J. Atmos. Sci*., **63**, 1231-1252.

Dowell, D.C., F. Zhang, L.J. Wicker, C. Snyder, and N.A. Crook, 2004: Wind and temperature retrievals in the 17 May 1981 Arcadia, Oklahoma, supercell: Ensemble Kalman filter experiments. *Mon. Wea. Rev*., **132**, 1982-2005.

Evensen, G., 1994: Sequential data assimilation with a nonlinear quasi-geostrophic model using Monte Carlo methods to forecast error statistics. *J. Geophys. Res*., **99** (C5), 10 143-10 162.

Gaspari, G., and S.E. Cohn, 1999: Construction of correlation functions in two and three dimensions. *Quart J. Roy. Atmos. Sci.,* **125**, 723-757.

Johns R.H., and W. D. Hirt, 1987: Derechos: Widespread Convectively Induced Windstorms. *Wea. Forecasting*, **2**, 32-48.

Kain. J.S., S.J. Weiss, M.E. Baldwin, G.W. Carbin, D. Bright, J.J. Levit, and J.A. Hart, 2005: Evaluating high-resolution configurations of the WRF model that are used to forecast severe convective weather: The 2005 SPC/NSSL Spring Experiment. Preprints, *21st Conf. on Weather Analysis and Forecasting*, Amer. Meteor. Soc., Washington, D.C. paper 2A.5.

Snyder, C., and F. Zhang, 2003: Assimilation of SImulated Doppler Radar Observations with an Ensemble Kalman Filter. *Mon. Wea. Rev*., **131**, 1663-1677.

Tong, M. and M. Xue, 2005: Ensemble Kalman Filter Assimilation of Doppler Radar Data with a Compressible Nonhydrostatic Model: OSS Experiments. Mon. Wea. Rev., 133, 1789-1807.

Weisman M.L., Skamarock, W. C., Klemp, J. B. 1997: The resolution dependence of explicitly modeled convective systems. *Mon. Wea,r Rev.*, **125**, 527–548.

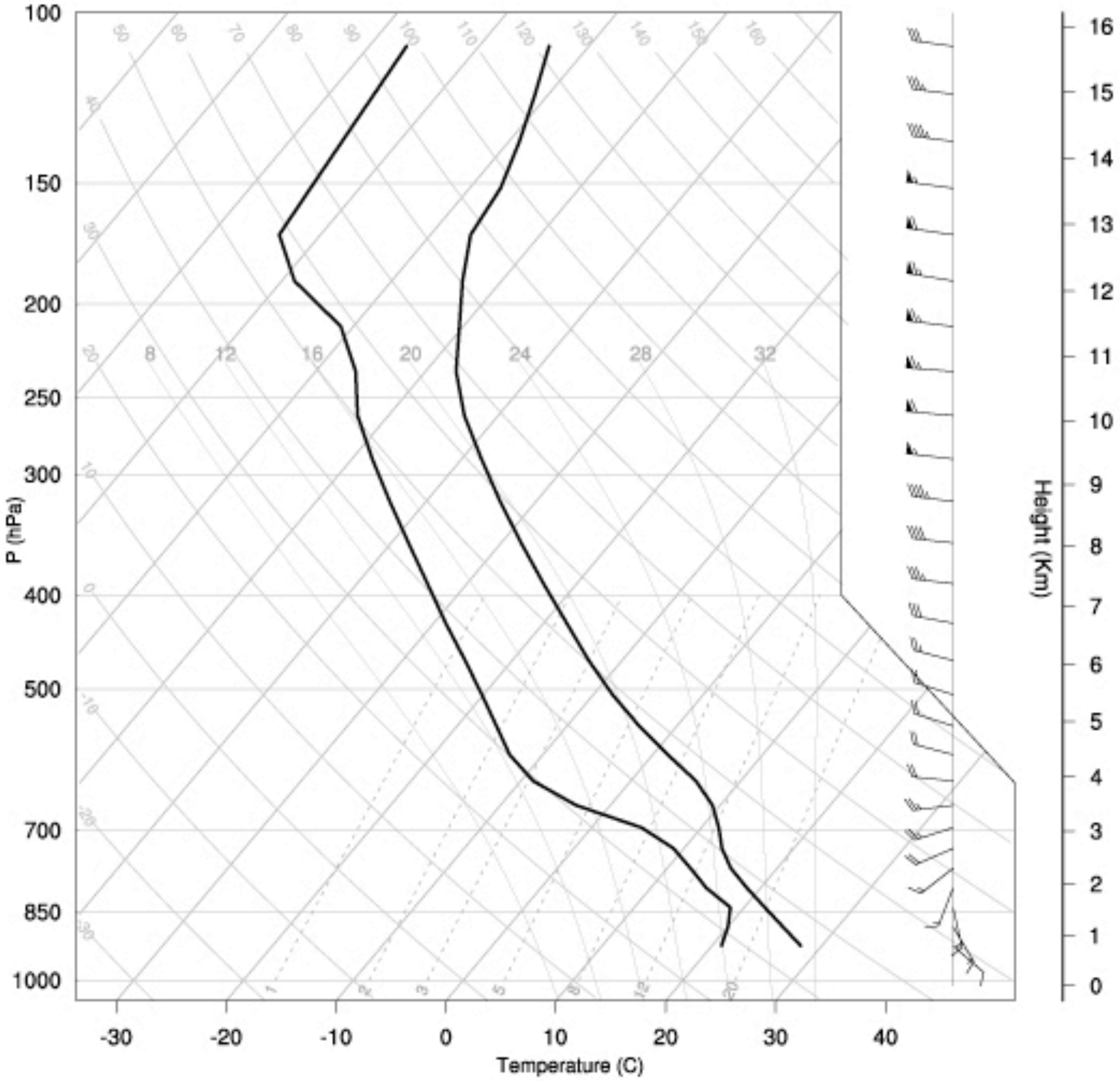

Fig. 1. RUC model sounding near Buffalo, OK valid at 2300 UTC 16 June 2005. Winds are in knots.

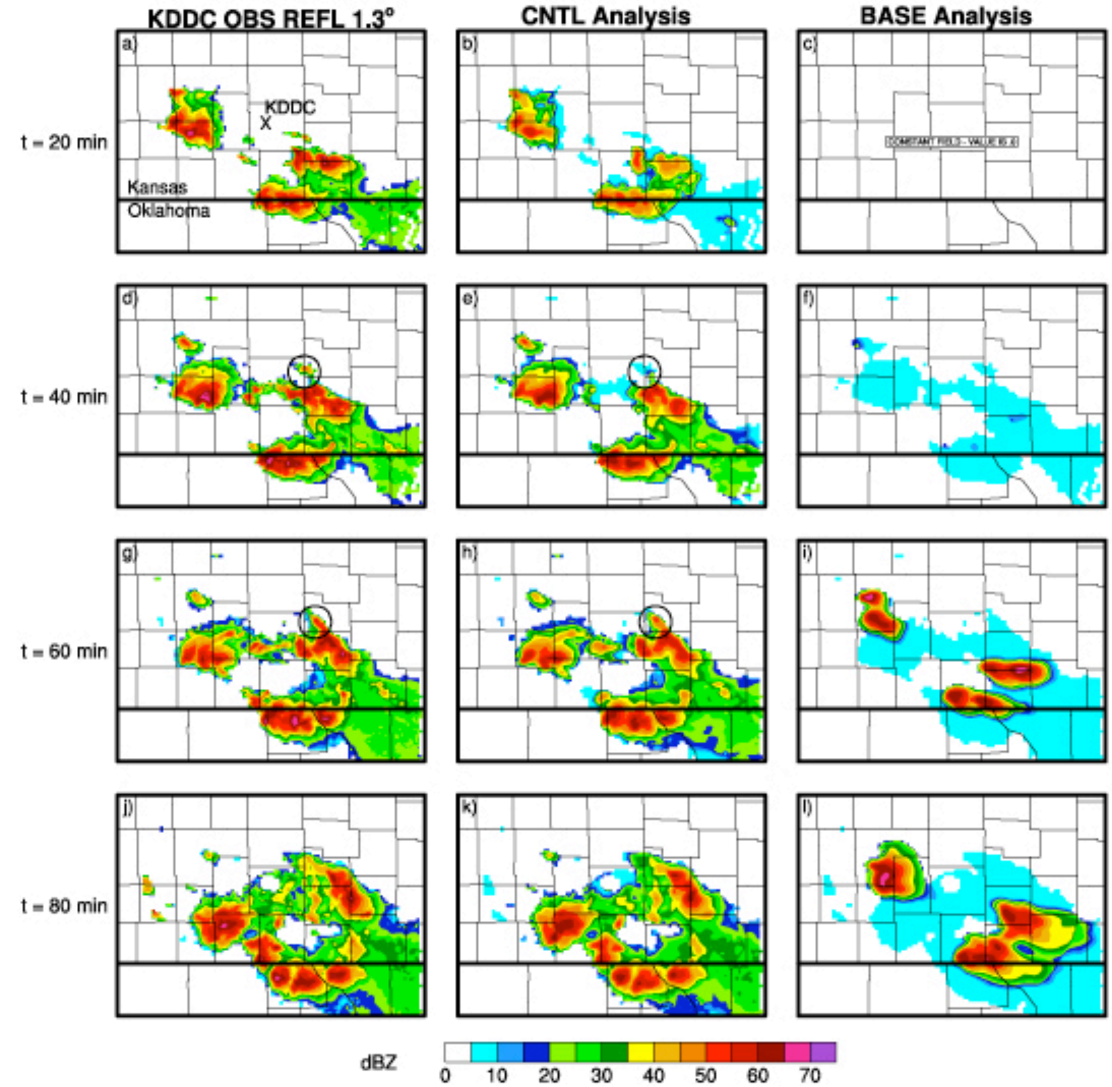

Fig. 2. A comparison of the observed 1.3° reflectivity from KDDC (leftmost column), the ensemble mean reflectivity from the control assimilation experiment (middle column), and the reflectivity from the baseline experiment (rightmost column) at 20 minutes (a-c), 40 min (d-f), 60 min (g-i), and 80 min (j-l) into the simulations. The location of the KDDC radar is indicated in 2a. The cells circled in d-e and g-h are discussed in the text. The model reflectivity is displayed on a conical surface that emulates a 1.3° scan from KDDC.

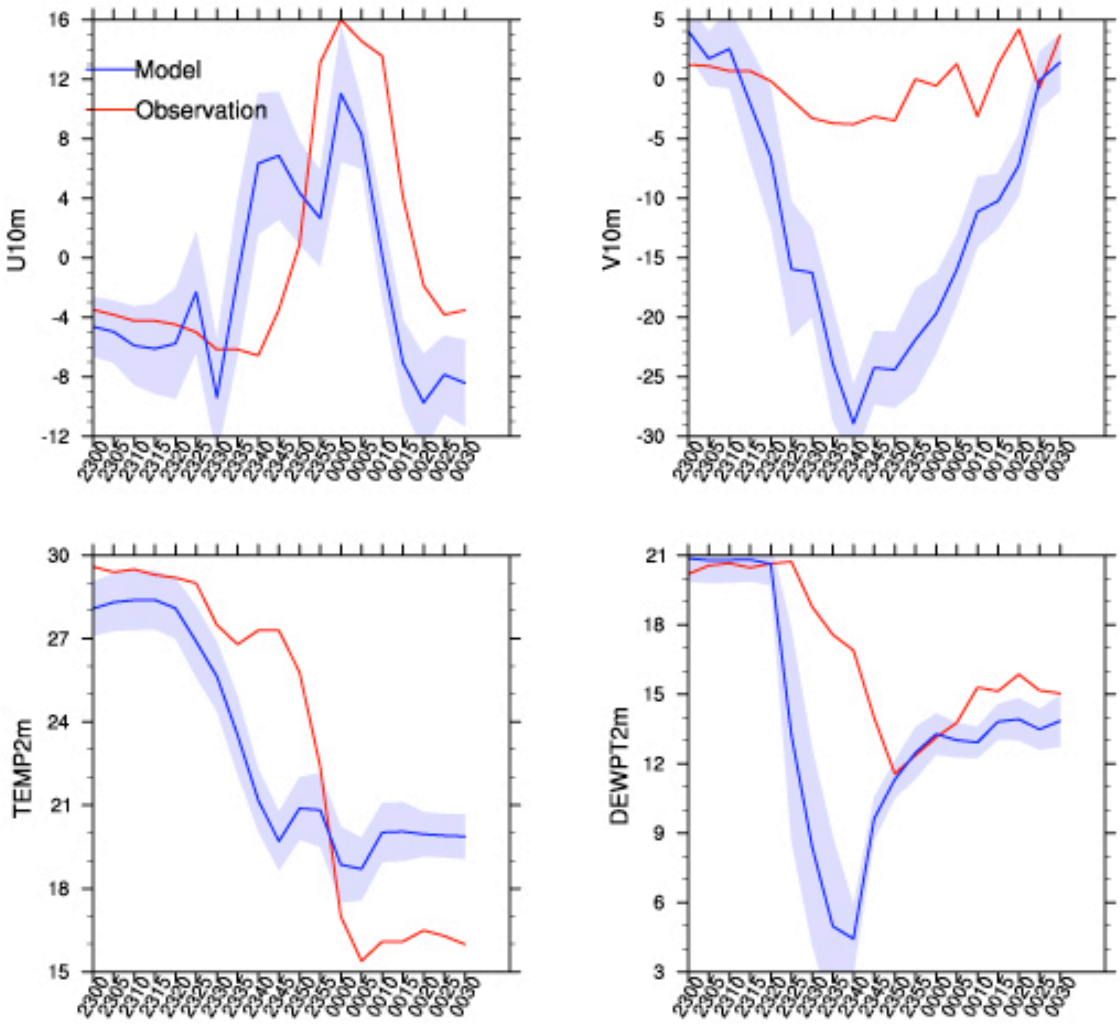

Fig. 3. A comparison of the observed and modeled conditions at the Oklahoma Mesonet site at Buffalo, OK from 2300 UTC on 16 June to 0030 UTC on 17 June. Observations are indicated by the red line for the 10 m u wind component (m s^{-1}, upper left panel), 10 m v wind component (m s^{-1}, upper right panel), 2 m temperature (C, bottom left panel), and 2 m dewpoint (C, bottom right panel). The thin blue line represents the ensemble mean and the surrounding blue shading represents the spread. Model values are at the lowest model level (125 m).

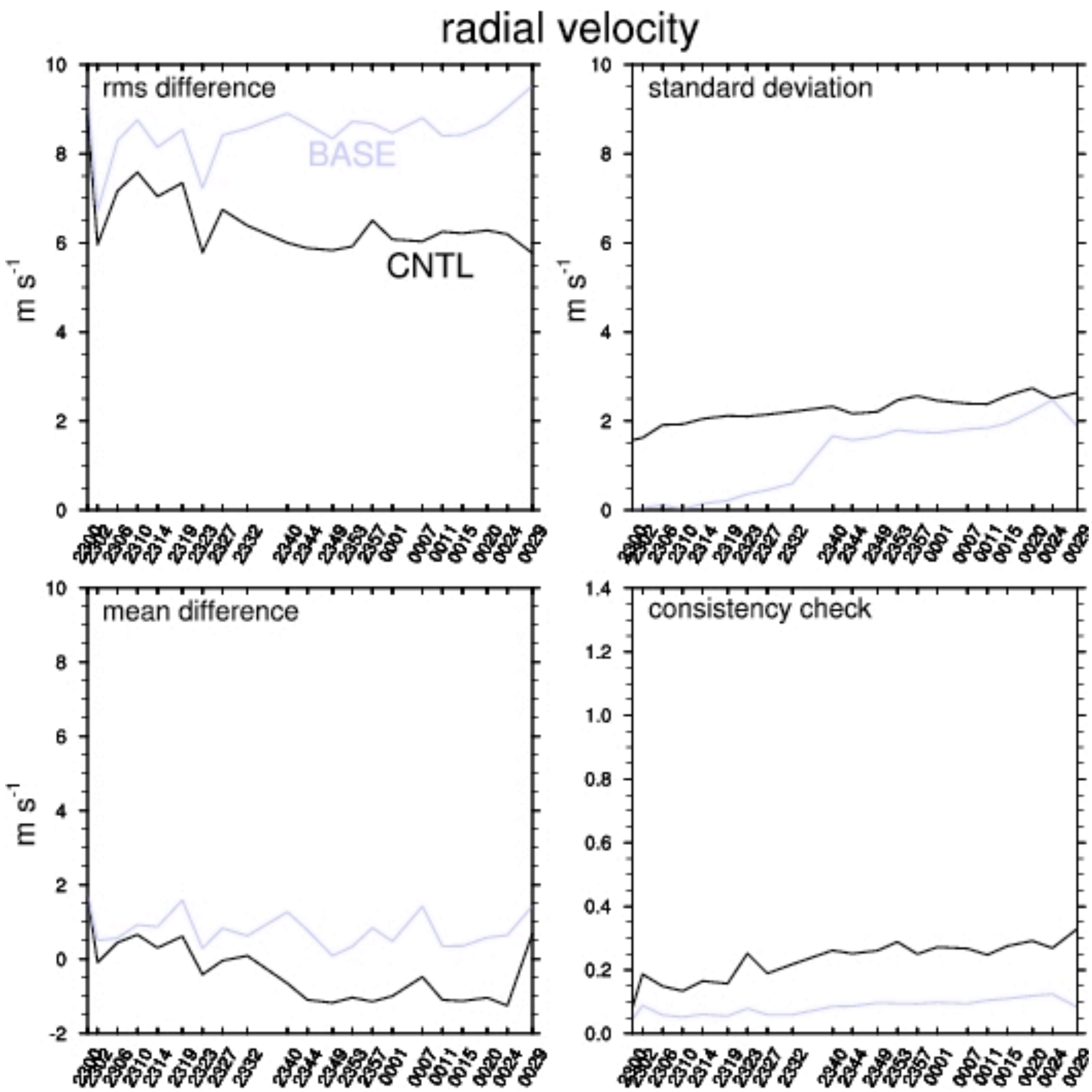

Fig. 4. Statistical evaluation of the BASE and CNTL experiments for radial velocity. The independent observations from KVNX are used as truth.

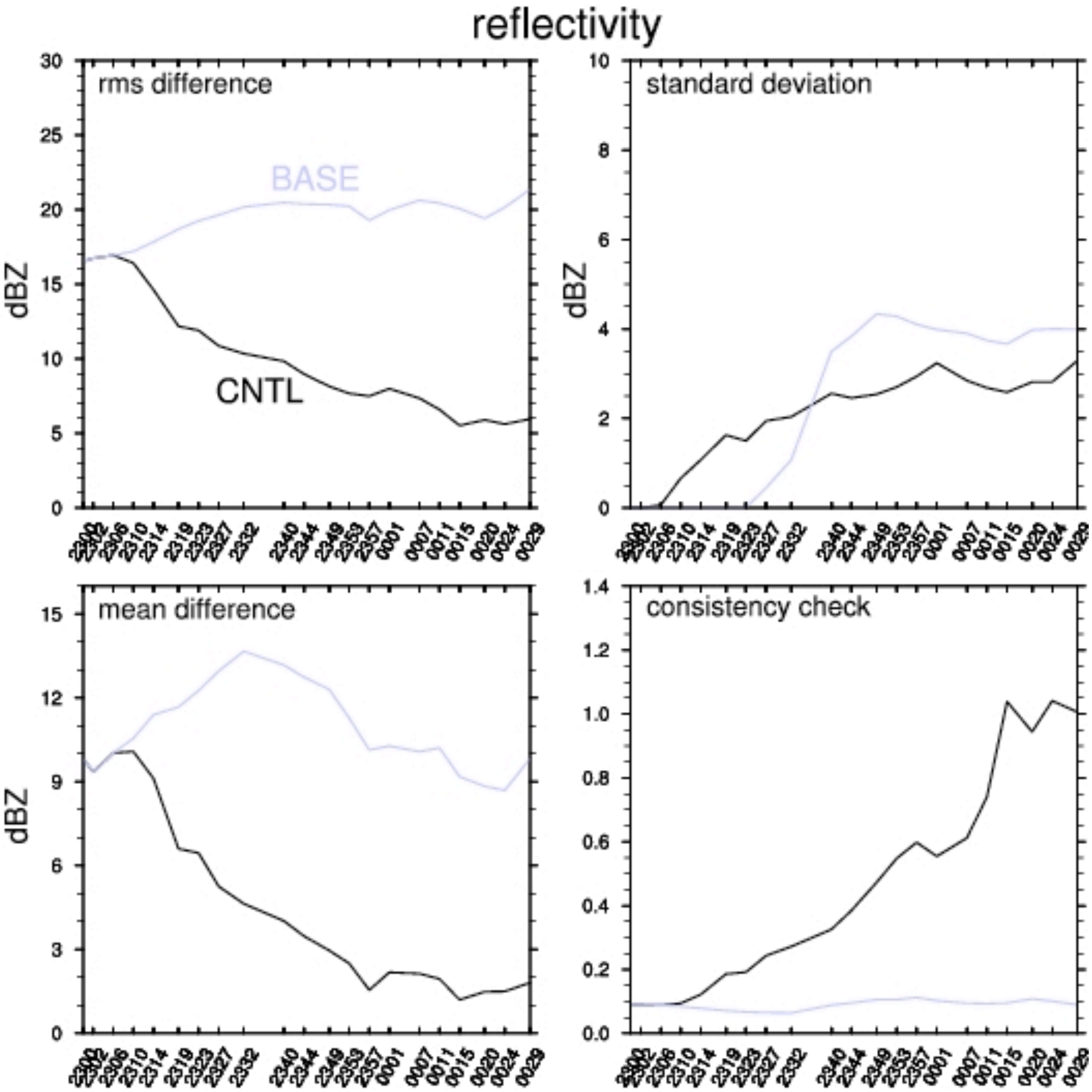

Fig. 5. Statistical evaluation of the BASE and CNTL experiments for radial velocity. The independent observations from KVNX are used as truth.

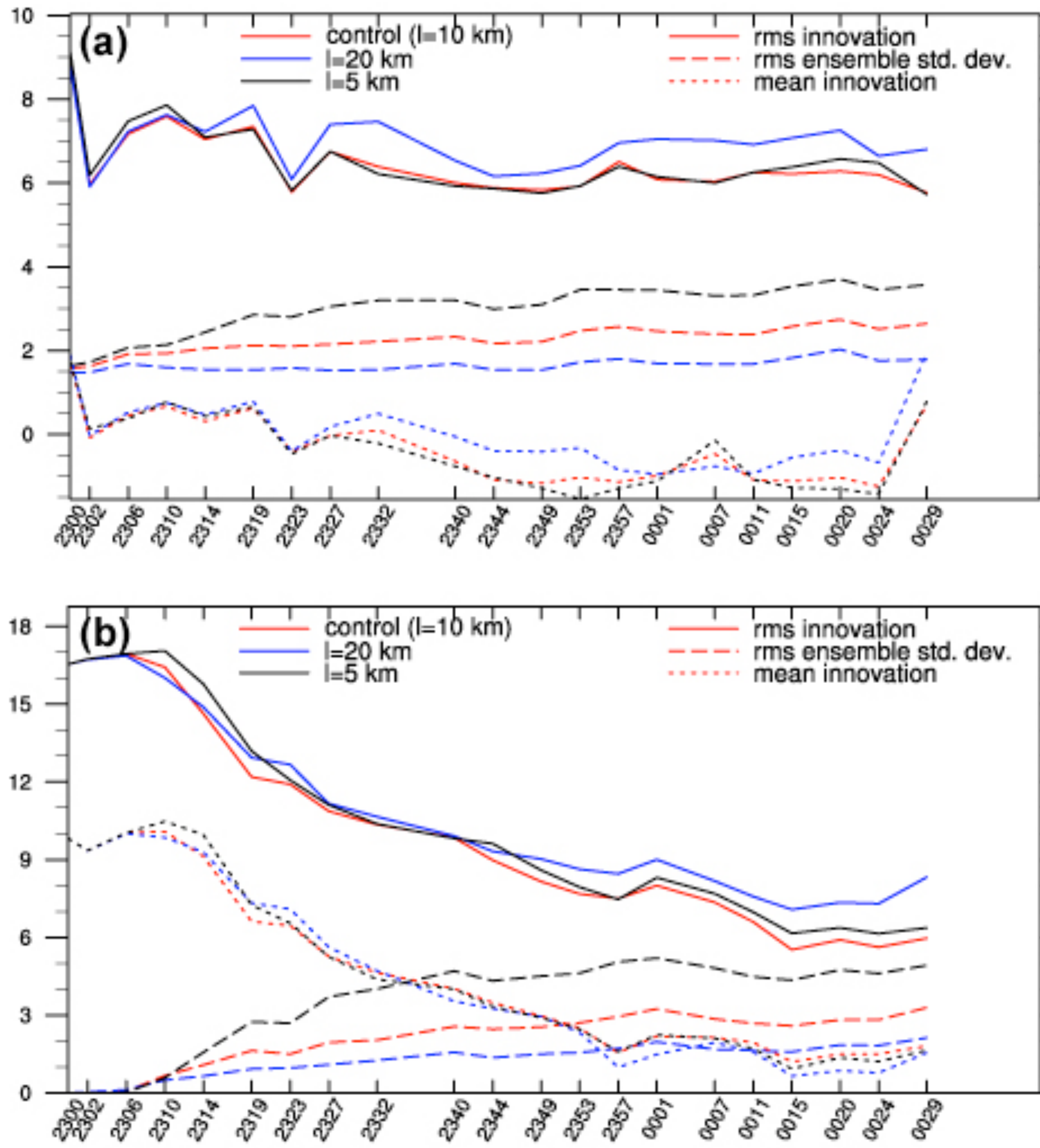

Fig. 6. Statistical evaluation of the CNTL (red), 20 km (blue), and 5 km (black) localization experiments for (a) radial velocity and (b) reflectivity. The independent observations from KVNX are used as truth.

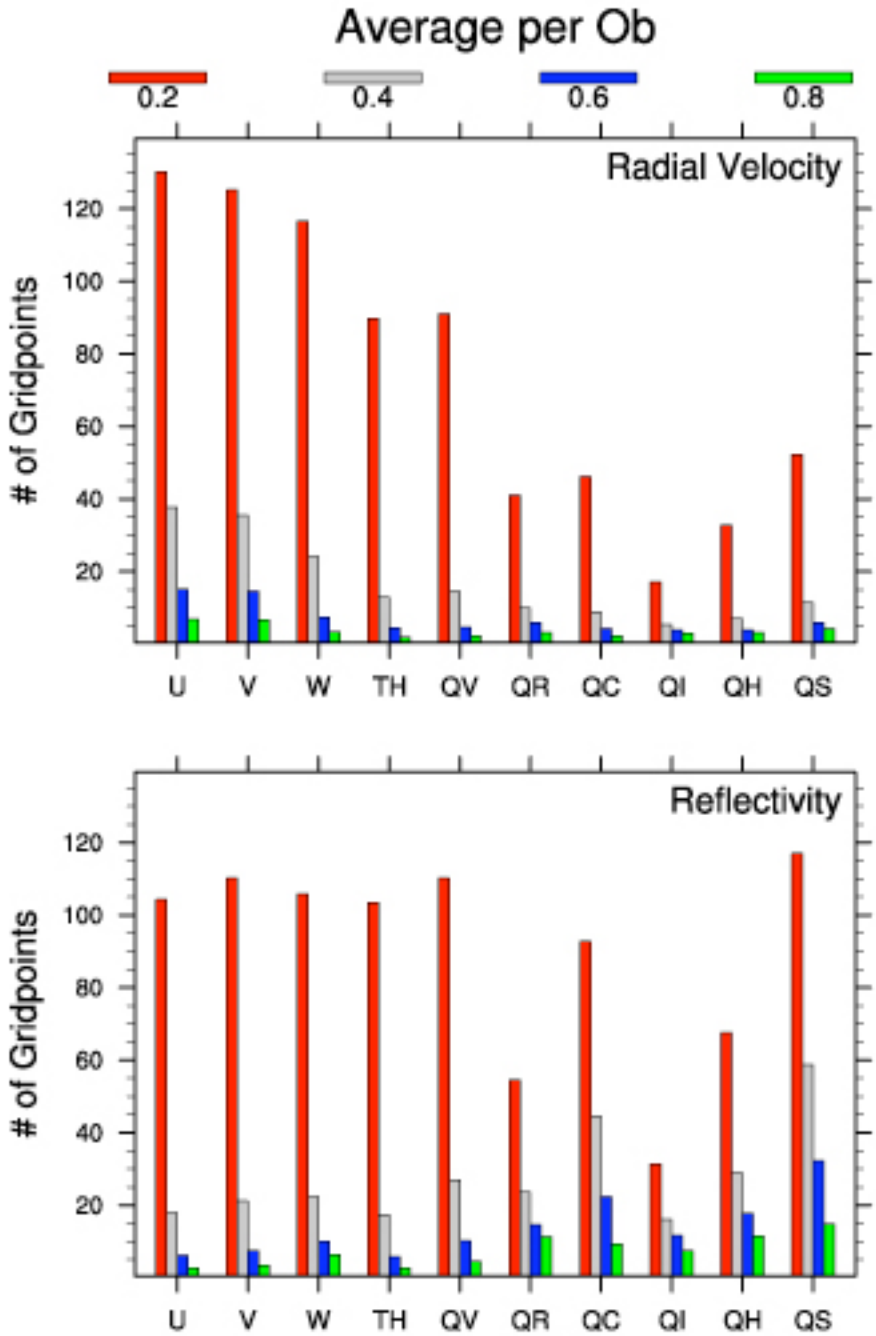

Fig. 7. Average number of grid points adjusted over the 90-minute assimilation period for each model variable (along x-axis) within the localization radius for the correlation threshold experiments (red="cor2", grey="cor4", blue="cor6", green="cor8"). Top panel is for radial velocity observations; bottom panel is for reflectivity observations. U, V, and W are the wind components, TH is perturbation potential temperature, QV, QR, QC, QI, QH, and QS are the water vapor, rainwater, cloud water, ice, hail, and snow mixing ratios, respectively.

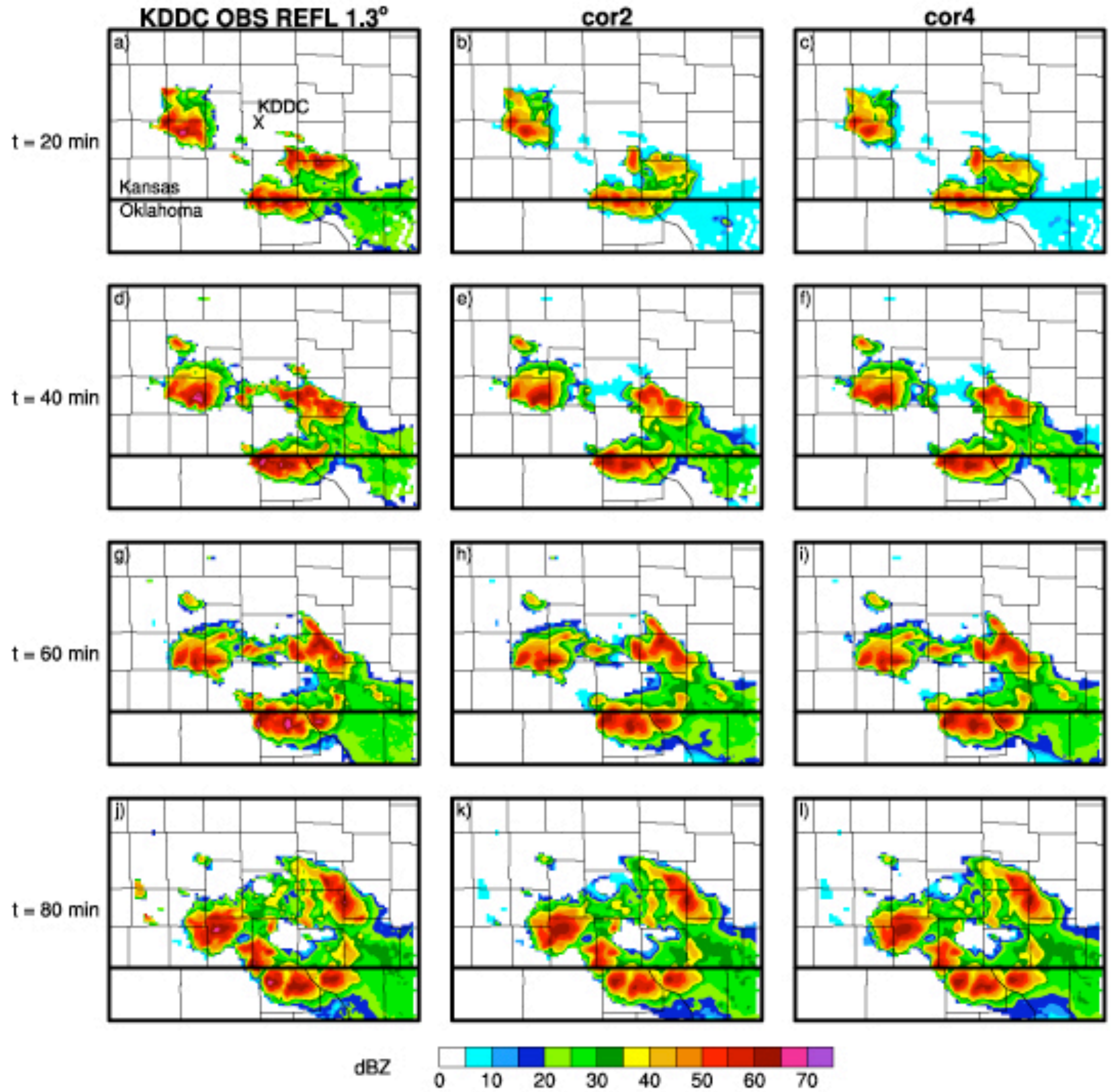

Fig. 8. As in Fig. 2, but for the cor2 and cor4 assimilation experiments.

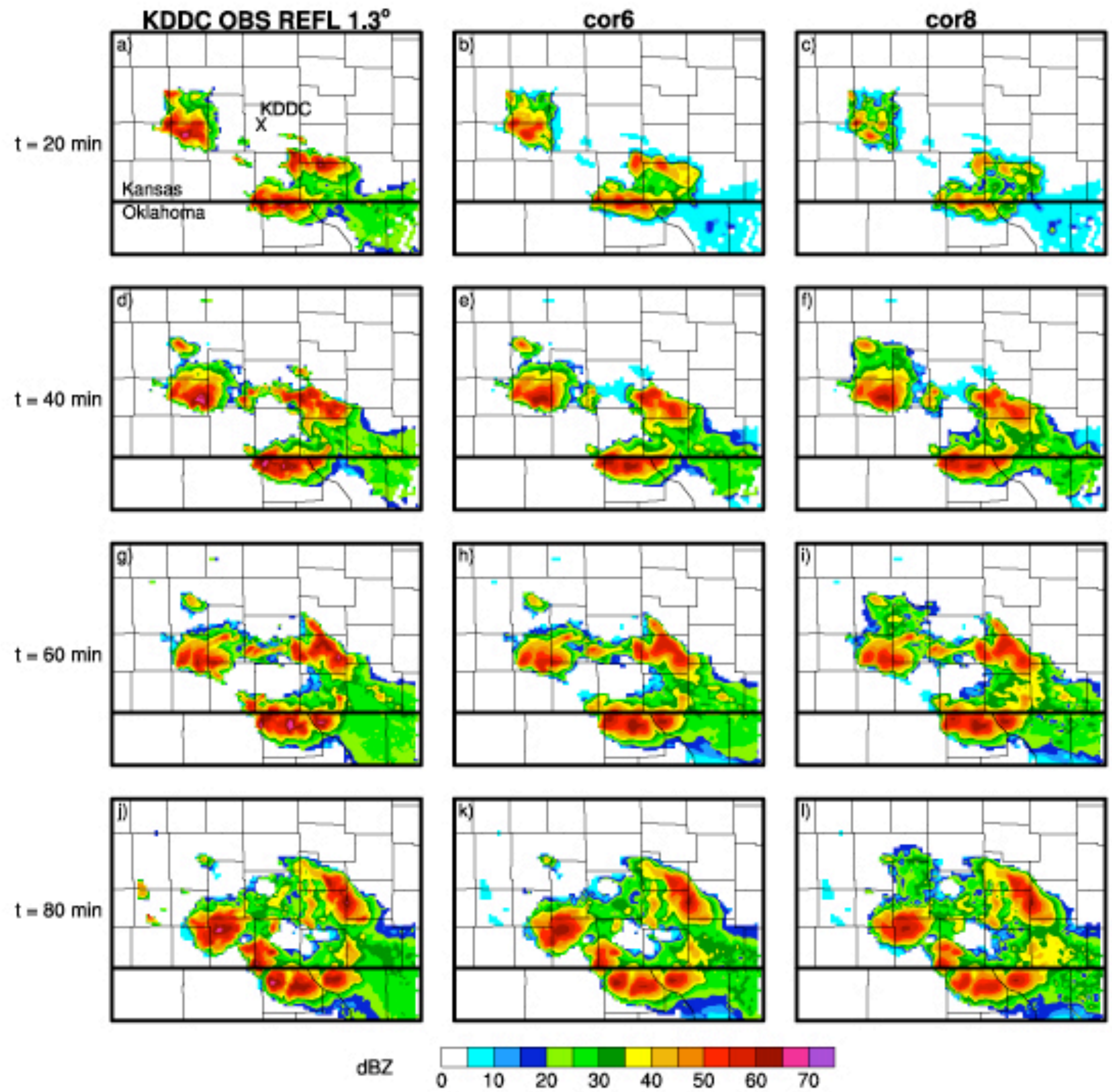

Fig. 9. As in Fig. 2, but for the cor6 and cor8 assimilation experiments.